Development of large fish farm numerical modeling techniques with in-situ mooring tension comparisons

David W. Fredriksson[a,*] Judson C. DeCew[b], Igor Tsukrov[c], M.R. Swift[c] and James D. Irish[d]

[a] Department of Naval Architecture and Ocean Engineering, United States Naval Academy, 590 Holloway Road, 11D Annapolis, MD 21402 USA

[b] Center for Ocean Engineering, University of New Hampshire, Durham NH 03824 USA

[c] Department of Mechanical Engineering, University of New Hampshire, Durham NH 03824 USA

[d] Department of Applied Ocean Physics and Engineering, Woods Hole Oceanographic Institution, Woods Hole, MA 02543 USA

Abstract

A study is conducted to validate a numerical model for calculating mooring system tensions of a large fish farm containing 20 net pens in the absence of waves. The model is forced using measured current velocity values obtained outside of the farm. Mooring line tensions calculated with the numerical model are compared with load cell field data sets. The approach considers current velocity reduction and load characteristics that occur through the net pen system for both clean and fouled net conditions. Without accounting for the reduction, the numerical model produces excessively conservative results. With reduction, a substantial improvement occurs. Understanding these differences will help to establish appropriate safety factors when designing large marine fish farms using the model. Additional validation studies should be conducted with wave and current forcing to investigate the modeling large fish farms for exposed or open ocean sites.

Keywords: mooring analysis, finite elements, flow reduction, fouled nets

*Corresponding Author, Tel.: +1 410 293 6434
fredriks@usna.edu (D.W. Fredriksson)
jcdc@unh.edu (J.C. DeCew)
igor.tsukrov@unh.edu (I. Tsukrov)
mrswift@unh.edu (M.R. Swift)
jirish@whoi.edu (J.D. Irish)

1. Introduction

The work presented in this paper represents a step in the evolution to develop engineering techniques for the design of large marine aquaculture systems. The techniques typically incorporate the use of numerical and physical models combined with field data sets and experience for validation purposes. Recent work has focused on the development of a fluid-structure interaction model using finite elements with hydrodynamic loading given by a version of Morison equation (Morison et al., 1950). In the model, Morison equation is modified to account for relative motion between the structural element and the surrounding fluid in both waves and currents. Implementation of the model is described by Gosz et al. (1996) where primary assumptions consider the aquaculture structures to be made of small diameter, smooth cylinders. Improvements to the original model include a better representation of the nets and the inclusion of nonlinear elastic elements, as described in Tsukrov et al. (2003) and Tsukrov et al. (2005), respectively.

A series of studies have also been done to explore the capabilities of the numerical model for engineering design applications. Experiments have been conducted comparing numerical model calculations with scaled physical model test results and field obtained data sets. Initial studies focused on the dynamics of a small (600 m^3), semi-rigid fish cage with a central spar construction. Validation studies were performed in both waves and currents as discussed in Fredriksson et al. (2003a) and Fredriksson et al. (2005). Palczynski (2000) and Fredriksson et al. (2003b) examined the steady drag characteristics of the small central spar cage. In these experiments, a numerical model and a 1:15.2 scale model of the fish cage were used in a series of computer simulations and tow tank tests, respectively. An open ocean drag test was also performed with the actual fish cage

and all the results compared. Both the physical model and field tests showed evidence of velocity reduction through the nets, which was not (initially) considered using the numerical model. This effect was also documented by Aarsnes et al. (1990) and Loland (1991) using theoretical and physical model approaches. For small fish cage and mooring systems, the velocity reduction may be small enough to be incorporated in the design load (Fredriksson et al., 2004). For modeling large commercial size fish farms, however, the velocity reduction effect needs to be considered to prevent over design.

The objective of this study is to develop the same numerical model to include horizontal flow reduction capability for improved representation of large marine fish farm systems. Since it is impractical to perform physical model tests of large fish farms, another objective is to validate the technique with field measurements. In this validation step, a field program was conducted at a large fish farm site without waves so that comparisons could be made considering only the steady drag components used in the numerical model. The improved model is forced using current velocity values measured at the fish farm site containing twenty net pens while in full operation. The modeling techniques consider the horizontal flow reduction using a simplified control volume approach for both clean and fouled net conditions. Simulations were performed and the calculated mooring system tensions were compared with those measured.

2. Fish Farm Particulars

The field study was performed at a fish farm located in Broad Cove near Eastport, Maine (USA), as shown on Figure 1. Broad Cove is connected to the Bay of Fundy where extreme tidal elevations create strong currents providing the dominant forcing on the farm structure. The farm is protected from waves of the Gulf of Maine by Campobello

Island (Canada). The fish farm contains 20 net pens in a 4x5 configuration (Figure 2). Each of the pens has a circumference of 100 meters and is connected to a near-surface mooring grid with 26 anchor legs. The net pens are made of High Density Polyethylene (HDPE) pipe with suspended nets. Broad cove has an average depth of approximately 15 meters with a tidal range of 8 to 9 meters. The mooring grid is located at a depth of approximately 5 meters and is supported with twenty-six 1.8 meter diameter steel flotation spheres. The anchor legs, which are mostly chain, extend down to the bottom beneath the floats and the grid. The dimensions of the farm, as contained by the mooring grid, are approximately 275 by 220 meters with individual square grid dimensions of 55 meters.

The net pen at the southwest corner of the farm was the primary focus area in this study since the incoming tidal currents generally come from the west and from the south (note on Figure 2 the southwest mooring components have double anchors). Instrumentation was deployed in the focus area to measure the wave influence on the farm, internal and external current velocities and mooring component tensions. Current meters and load cells were deployed during three operational conditions, when (1) clean containment and predator nets for smolts, (2) clean containment and predator nets for standard grow out and (3) containment and predator nets that were fouled were installed. The third condition occurs at the end of the stocking schedule (at approximately 16-18 months). In this study, data sets from the clean and fouled net conditions were used for comparison purposes. Different net dimensions and levels of fouling will have different flow field and mooring tension distribution characteristics. Using measured current velocities as input, numerical model simulations were performed with and without current velocity

reduction for clean and fouled nets. Calculated results were then compared with load cell measurements.

3. Field Measurements

3.1. Instrumentation

The goals of deploying field instrumentation were to (1) verify that waves were small at the fish farm site, (2) obtain current velocities to be used as input to the numerical model for clean and fouled net conditions, (3) obtain current velocities to estimate the reduction through the southwest net pen and (4) obtain anchor leg tension response for comparison with numerical model calculations for clean and fouled net conditions.

To verify that the influence of wave forcing at the fish farm site was negligible, an Acoustic Doppler Current Profiler (ADCP) with wave processing software (see www.rdinstruments.com) was installed from October 3, 2003 until January 5, 2004. The ADCP was deployed outside of the farm in the southwest direction. The relative position with respect to the southwest net pen is shown on Figure 3. The ADCP was moored up off the bottom in an average depth of 25 meters. The instrument was configured to measure waves at the beginning of each hour for twenty minutes at a rate of 2 Hz. The instrument provides wave spectral estimates inferred from velocity profile, pressure and surface slope measurements.

Current velocities used as input to the numerical model were obtained using a Nortek AQUADOPP current meter (see www.nortek-as.com). This current meter was located at an external farm location approximately 23 meters from the southwest net pen. To estimate the velocity reduction through the southwest net pen, a MAVS current meter (see www.nobska.net) was installed at an internal farm location approximately 23 meters

behind the net pen. A detailed schematic of the southwest net pen is shown on Figure 3 where the current meter positions are indicated. Both current meters were attached to the mooring grid, which moved up and down with the tides, keeping both current meters about 4 meters below the surface. This position is about the mean depth of the net pens. Using these instruments, three minute averages of the current velocity were measured every 20 minutes. The current meters were deployed from October 3, 2003 to December 31, 2003 for the fouled net condition and from June 7, 2004 to September 22, 2004 for the clean net condition.

The field measurement plan also included the deployment of five, 90 kN capacity load cells on anchor legs around the southwest net pen (also shown on Figure 3). Four additional load cells, with the capacity of 44 kN, were connected to the net pen attachment lines. The loads from the 44 kN capacity load cells were used as part of a companion study examining net pen structure capabilities (Fredriksson et al., in preparation). The 90 kN capacity load cells were attached to the west (W), southwest-west (SW-W), southwest-southwest (SW-SW), southwest-south (SW-S) and south (S) anchor legs. In this study, the data sets from these instruments were considered for comparison with numerical model calculations. The anchor load cells were deployed during the clean and fouled net conditions. During each deployment, the instruments were set to record at a rate of 5 Hz for 20 minutes each hour. This sampling scheme was chosen so that if wave forcing was strong, it would be observed. The load cells were deployed from October 3, 2003 to December 31, 2003 for the fouled net condition and from June 8, 2004 to September 22, 2004 for the clean net condition. Additional instrumentation and field deployment details are provided in Fredriksson et al. (2006).

3.2. Field Data Set Results

During the three months that the ADCP was deployed, few substantial wave events were observed. Results that were obtained showed that energy-based significant wave heights at the Broad Cove site were less than 1 meter with dominate periods less than 3 seconds. For example, during one of the wave events that occurred on October 28, 2003 at 0200 UTC, the energy-based significant wave height and dominate period was estimated to be 0.8 meters and 2.2 seconds, respectively. These waves may influence the dynamics of smaller farm components, such as the surface buoys, but the affect on mean anchor leg tensions was negligible. This data set is further discussed below.

The next step was to obtain current velocities to examine forcing input parameters and the corresponding anchor leg tensions for the clean and fouled net conditions for model validation. Data sets from the AQUADOPP and the load cells were examined according to the following criteria.

1. The current velocity must be in the northerly direction (between 315^{o} and 45^{o}) so that the southwest portion of the grid is tensioned.

2. The current velocity must have a constant heading maintaining direction for 20 minutes before and after load cell data sampling (although the magnitude of the current can be different). This will help insure that the system is set back against the current and a steady state loading condition is occurring.

3. The magnitude of the current velocity should be large enough to have a measurable affect on the tension in the mooring and net pen attachment lines. A value of approximately 0.25 m/s was qualitatively shown to be effective.

4. Tension measurements from the load cells should have values that are relatively steady for the first or last three minutes of the data set to help insure the system was in a steady state condition.

Current meter and mooring tension values were identified, using these criteria, for the

clean net condition on July 28, 2004 at 2100 UTC and for the fouled net condition on October 28, 2003 at 0200 UTC. The current meter values are summarized in Table 1. Included in the table are the date, time and current velocity characteristics for twenty minutes before, at and after the hour showing consistent magnitude and direction values. The current velocity information shown is also provided as east- and north-going components. The model input velocity was taken as the average between the measurements obtained at and twenty minutes past the hour. These values are also provided in Table 1.

For each load case, twenty minutes of tension data were obtained from the load cells. For the clean nets, data sets were acquired from the West, SW-W, SW-SW, SW-S and South anchor legs. For the fouled nets, data sets were acquired from the West and South anchor legs. The best data sets, however, were from the South and SW-S load cells since the currents were coming from that direction. For the fouled net condition, only information from the South anchor was used since water intrusion occurred in the SW-S instrument. The tension time series results from these three data sets are shown on Figure 4. Recall that on October, 28 2003 at 0200 UTC a wave event occurred producing an energy-based significant wave height of 0.8 meters and dominant period of 2.2 seconds. These waves created oscillating tensions recorded by the load cell as shown on the detailed plot on Figure 4. The data shows that wave influenced values do not affect the mean tensions.

The velocity data sets from the AQUADOPP and MAVS current meters were also examined to estimate the flow reduction through the southwest net pen for both the clean and fouled net conditions. A full discussion of the processing techniques is provided in Fredriksson et al. (2006) with the key points summarized here. Since the spatial and

temporal differences between the point measurements were substantial, velocity reduction was characterized from a variance perspective with measurements obtained over multiple tidal cycles. The measured north- and east-going velocity data sets from each of the current meters were processed to obtain a variance spectrum for both external and internal positions for each net condition. In the frequency domain, the component variance spectra were added to obtain the total horizontal velocity variance spectra. The area under the spectral curves, equal to the variance, was then found from which root mean square (RMS) velocities (U_{RMS}) were calculated. The variance and RMS velocity values are provided in Table 2. This can be considered assuming that the standard deviation is biased and the mean is zero. The U_{RMS} values for the external and internal locations were then used to obtain a percent reduction across the southwest net pen (from a variance perspective). The percent reduction values are also provided in Table 2. Note that in the Table, results for the smolt net deployment (condition 2) are also included, though not thoroughly discuss in this paper.

3.3. Simplified Control Volume Analysis

For the numerical model simulations, velocity reduction estimates were needed, not just for one net pen, but through the entire farm. Velocity reduction characteristics were estimated using a simplified control volume analysis. The approach seeks to estimate drag coefficient values for net pens for clean and fouled net conditions. The procedure was also performed for the smolt net condition. The analytical approach is similar to that described in Plew et al. (2005), where a technique was applied to a farm consisting of numerous hanging mussel droppers with diameters 10-20 cm. In this case, the farm consists of twenty, evenly spaced cylindrical net pens each with a diameter of 31.8 meters. The approach assumes uniaxial flow into a rectangular fixed control volume.

One end faces the incident current, while the other is interior to the distribution of net pens.

The approach assumes that the summation of forces in the direction of the flow can be estimated if the flow is steady and only one entrance and exit is considered,

$$\sum \left(F_x\right)_{on\ the\ fluid} = \dot{m}\left(U - U_o\right), \tag{1}$$

where the left side of the expression consists of the drag induced by cylindrical net pens and the right side is the change in momentum flux. In equation (1), $\dot{m}$ is the mass flow rate and U_o and U are the incoming and exiting velocities, respectively. The drag term can be expressed as

$$\sum \left(F_x\right)_{on\ the\ fluid} = -nF_d \Delta x W = -n\left[\frac{1}{2} C_d \rho D d_c U^2\right]\Delta x W \quad , \tag{2}$$

where: n is the number of net pens per area,
F_d is the drag force on one pen,
Δx is the control volume horizontal dimension in the direction of flow,
W is the control volume horizontal dimension perpendicular to the flow,
C_d is the drag coefficient,
ρ is the fluid mass density
d_c is the net pen depth and
D is the net pen diameter.

The change in momentum flux can be considered as

$$\dot{m}\left(U - U_o\right) = \dot{m}\left(U + \Delta U - U\right) = \left(\rho W d_c U\right)\Delta U \ . \tag{3}$$

By substituting equations (2) and (3) into (1), rearranging terms and by taking Δx and ΔU as differential forms as limits approach zero, the following expression can be obtained,

$$\int_0^x \frac{-nC_d D}{2} = \int_{U_o}^{U} \frac{du}{u} \ . \tag{4}$$

Equation (4) is evaluated for the drag coefficient for the three net conditions where the values for U_o and U were obtained from measured data sets where the total variance of

the horizontal velocity vector was calculated at external and internal farm locations. The value for n was taken as the number of pens divided by the width of the farm normal to the flow and by horizontal distance Δx.

Once the drag coefficient is obtained using the measured flow characteristics through 1 net pen, equation (4) can be rearranged such that,

$$U = U_o e^{\left(\frac{-nCdDx}{2}\right)} \tag{5}$$

and the velocity reduction through successive layers of pens calculated as a function of x.

Using the external and internal RMS velocity values and the control volume analytical approach, the flow reduction through multiple layers of net pens were examined. Using equation (4), the coefficient of drag, with respect to one layer of pens, was estimated for the three net conditions. Once the coefficient of drag was obtained, the calculation was performed through multiple layers of net pens to estimate the horizontal (diagonal) velocity through the farm using equation (5).

The reduction through the farm is modeled piece-wise assuming that the energy loss occurs as the flow passes through the net pens (Figure 5). In the Figure, U is the velocity at a particular distance x and U_o is the estimated external velocity. Also included on the Figure are the measured velocity reduction percentages obtained from U_{RMS} values from which the net pen drag coefficients are obtained. It should be noted that these calculations were performed assuming that the flow encounters the farm at approximately 45^o. The normalized results shown in Figure 5 were applied to the measured averages from Table 1 to obtain velocity values at various locations behind multiple net pens throughout the fish farm. The corresponding east- and north-going velocity reduction

components used as input to the numerical model simulations are provided in Table 3.

4. Numerical Modeling

4.1. Theoretical Review

Numerical model simulations were performed using a finite element computer program. The program employs a modified version of Morison equation (Morison et al., 1950) to calculate hydrodynamic forces on structural, truss-like elements. Following Haritos and He (1992), Morison equation is modified to account for the relative motion between the structural element and the surrounding fluid. The fluid force per unit length is represented as

$$\mathbf{f} = C_1\mathbf{V}_{Rn} + C_2\mathbf{V}_{Rt} + C_3\dot{\mathbf{V}}_n + C_4\dot{\mathbf{V}}_{Rn}, \qquad (6)$$

where $\mathbf{V}_{Rn}$ and $\mathbf{V}_{Rt}$ are the normal and tangential components of the fluid velocity relative to the structural element, $\dot{\mathbf{V}}_n$ is the normal component of total fluid acceleration and $\dot{\mathbf{V}}_{Rn}$ is the normal component of fluid acceleration relative to the structural element. The coefficients in equation (6) above are given by $C_1 = \frac{1}{2}\rho_w D C_n V_{Rn}$, $C_2 = C_t$, $C_3 = \rho_w A$ and $C_4 = \rho_w A C_a$, where D and A are the diameter and the cross-sectional area of the element in the deformed configuration, ρ_w is the water density, C_n and C_t are the normal and tangential drag coefficients. Coefficients C_3 and C_4 represent the inertial force components due to the fluid acceleration where C_a is the added mass coefficient. Note that C_n and C_a are dimensionless, while C_t has the dimension of viscosity.

The numerical procedure calculates C_n and C_t, using a method described by Choo and

Casarella (1971) that updates the drag coefficients based on the Reynolds number (Re_n) as follows

$$C_n = \begin{cases} \dfrac{8\pi}{\mathrm{Re}_n\, s}\left(1 - 0.87 s^{-2}\right) & \left(0 < \mathrm{Re}_n \le 1\right), \\ 1.45 + 8.55\,\mathrm{Re}_n^{-0.90} & \left(1 < \mathrm{Re}_n \le 30\right), \\ 1.1 + 4\,\mathrm{Re}_n^{-0.50} & \left(30 < \mathrm{Re}_n \le 10^5\right) \end{cases} \tag{7}$$

$$C_t = \pi\mu\left(0.55\,\mathrm{Re}_n^{1/2} + 0.084\,\mathrm{Re}_n^{2/3}\right) \tag{8}$$

where $\mathrm{Re}_n = \rho_w D V_{Rn} / \mu$, $s = -0.077215665 + \ln\left(8/\mathrm{Re}_n\right)$ and μ is the water viscosity. The coefficients C_1, C_2, C_3 and C_4 can be calculated assuming that the structural elements are smooth circular cylinders or modified to represent the hydrodynamics of other element types such as non-cylindrical buoys or nets. For example, Tsukrov et al. (2003) use this approach to develop the *consistent net element*.

The model also incorporates the buoyancy, weight, inertia and elastic forces of the element. Introducing linear finite elements with two nodes having three degrees of freedom (nodal displacements) each, the forces are discretized using a shape function matrix so that the forcing components on each element can be integrated over the length of the element (see Gosz et al. 1996). The standard finite element discretization of the structural system in a moving fluid environment results in the following system of differential equations,

$$\left(\mathbf{M} + \mathbf{m}\right)\ddot{\mathbf{q}} + \mathbf{C}\dot{\mathbf{q}} + \mathbf{K}\mathbf{q} = \mathbf{R} + \mathbf{H} \tag{9}$$

where $\mathbf{q}$ is the (time dependent) vector of nodal displacements, $\mathbf{M}$ is the time independent consistent mass matrix, $\mathbf{m}$ is the virtual mass matrix, $\mathbf{C}$ the damping matrix

(due to fluid drag), **K** is the global stiffness matrix (which can be expanded into a tangent stiffness matrix and internal force vector), **R** is the equivalent nodal force vector due to gravity and buoyancy forces and **H** is the equivalent nodal force vector due to wave and current loads.

In the model, equations (9) are discretized in time and integrated using the Newmark-Beta method. The Newton-Raphson iteration scheme is employed to find nodal displacements at every time step from which velocities, accelerations and stresses are obtained. The model also includes a non-linear Lagrangian formulation to account for large displacements of structural elements. In this study, the model represented by equations (9) is used without wave input and results analyzed for steady state conditions to focus on the fluid drag contribution.

4.2. Implementation of Flow Reduction in the Model

Additional code modifications were necessary to model the drag forces on the farm represented as the horizontal flow changes due to net conditions and levels of fouling. These modifications included corrections to coefficients C_1 and C_2 by adjusting V_{Rn} (and therefore the Reynolds number). A similar approach was utilized by Fredriksson et al. (2005) to account for possible vertical stratification of *in-situ* flows. Previous modeling studies of large fish farm systems applied the same horizontal environmental conditions to all of the elements, regardless of wake effects or blockage that may be occurring. This approach has worked reasonably well when applied to small farms in open ocean conditions where limited velocity reduction occurs (Fredriksson et al., 2005). The farm examined here, however, is presently the largest structure ever simulated using the model. Since evidence of significant horizontal current reduction exists, it was

hypothesized that the change in current within the farm would significantly affect the tensions calculated by the model.

Two approaches were considered to account for the horizontal velocity changes. The first was to develop a new element that incorporates a specific velocity reduction characteristic. This approach was used with a certain degree of success, but only a single fish cage was modeled (Fredriksson et al., 2003b). For the large farm, however, this "reduced velocity" element would have to be generated for each existing element type (truss, buoy, net, etc) increasing the number used in the model. In addition, if multiple velocity reduction locations exist, even more element types would be required, which would further reduce the computational efficiency. The second approach, adopted in this study, was to allow multiple horizontal current profiles to be generated and applied to specific elements. Therefore, several different current values could be applied to different elements. If the current reduction is known, it can be incorporated into the model.

The code was modified to accommodate up to 25 horizontal profile points. This would allow for a variety of applications to be investigated and, if needed, a large current reduction in a complex system. The program produces a specifically generated file, which contains the current (velocity, depth) information for each horizontal profile. The proper profile is then assigned to the associated element for processing. This repeats for each element at each time step. Modifying the code in this manner allows for the most versatile use of the model, without compromising the efficiency of the program. This could be expanded into three-dimensional spatial matrix of velocity vectors with higher resolution, possibly generated by validated computational fluid dynamic models.

4.3. Geometric and Material Properties

To build the numerical model of the entire net pen and mooring system, the geometric and material properties for each component were determined. The net pen is comprised of surface and submerged rings made of HDPE and connected vertically by predator and containment nets. One of the modeling input parameters is the net solidity used with the *consisted net element* (Tsukrov et al., 2003). In this context, solidity is defined as the ratio between the projected and total outline area of a flat net panel. The nets are nylon, have knotless construction and are treated with antifouling paint, typical of the industry standards in the region. The general net characteristics, which include the twine diameter, net spacing and solidity estimates are provided in Table 4. Data sets collected during the clean and fouled net conditions were of particular interest in this study because they represent the least and most blockage, respectively. For the clean net condition, the solidity is taken as the superposition of both the predator and containment net values provided in Table 4. For the fouled net condition, however, solidity was difficult to quantify in the field and therefore estimates were made.

To estimate the solidity for the fouled nets, the information on Figure 5 was used where the velocity reduction was found to be a function of net pen solidity. The solidity for the smolt and clean nets were measured from actual net samples and were 0.408 and 0.197, respectively. Using normalized reduction values from the measured field data results through one net pen and the respective total solidity, a linear curve fit was applied to estimate the solidity for the fouled case. The linear curve fit included conditions where the solidity could be equal to 1 and 0. Using this technique, an estimated solidity of 0.588 was found for the fouled condition. The net solidity values and the other geometric and material properties of the pen are provided in Table 5.

The geometric and material properties were also determined for the mooring system and used as input to the model. These values are provided in Table 6. The primary components consist of anchor and buoy chain, grid lines, buoys and connector plates.

4.4. Numerical Modeling Results

Using the measured current velocities as input and the geometric and material properties to build the model, numerical simulations were performed with and without current velocity reduction for net solidity values estimated for the clean and fouled net conditions. The mooring tension distributions (kN) are shown on Figures 6 and 7 superimposed on a non-deformed plan view of the fish farm model for the clean and fouled net conditions, respectively. On the Figures, mean values calculated without reduction are underlined, while values calculated with reduction are in bold. The computer model also provides the entire grid and net pen attachment line stresses from which tensions can be calculated. These values are not included on the Figures for clarity purposes. The anchor leg locations of particular interest and the forcing current velocity vector components are also shown on the Figures.

5. Discussion

The mean and maximum values from the South and SW-S anchor load cells are provided in Table 7 for each net condition. The results show that on the South anchor, for clean and fouled net current velocities of 0.285 and 0.231 m/s, mean tensions were 24.5 and 21.1 kN, respectively. The numerical model calculations, using the same current velocities as input and employing the velocity reduction schemes, produced South anchor tensions of 34.5 and 22.4 kN (also provided in Table 7). Measured values for the SW-S anchor yielded a mean tension of 14.6 kN, compared with the calculated result of 16.3

kN. In general the model over predicted the tensions in the mooring lines, but not by an unreasonable amount. When further examining the numerical model results, it is clear that the values obtained by employing the flow reduction estimates are substantially better than those obtained without reduction, where values were as much as 160% higher. Understanding these differences will help to establish safety factors when designing large marine fish farms using the model.

Other areas of further work exist, however, to refine the design process using the numerical model. For example, the results presented do not consider the non-uniform deployment of the mooring, which can also affect system tensions as described in Rice et al. (2006). In this case, the geometry of the system in the model was built symmetrical.

Another important consideration is the velocity reduction scheme. The estimates provided using the simplified control volume approach are obtained from velocity variances and do not consider three dimensional continuity effects at both the net pen and farm scales. Reduction values through multiple net pens may be over-estimated. Another factor that may have affected the results is the position of the external current meter, which may not have been far enough away from the influence farm. Future studies should also include the affect of the stocking densities on the flow field.

6. Conclusion

Employing the horizontal flow reduction modeling capability is an important step in the development of techniques used to design large marine fish farm systems. Special attention will also be necessary if this numerical model is to be used for the design of similar farms in exposed conditions that contain multiple frequency wave fields. Though the Morison equation approach used in the model calculates wave drag and inertial

forces, it does not consider diffraction effects. Additional validation studies should be conducted so that model users better understand calculated results in this application.

In addition to the engineering of fish farm structural components, environmental aspects must also be considered. Results imply that the placement of fish farms in protected sites affect the hydrodynamics of the natural environment. Reduced velocities will also influence the exchange of oxygen and the transport of wastes. Quantifying these parameters must be understood to optimize growth rates and to better assess environmental impact. Utilization of validated computational fluid dynamic techniques, as introduced by Patursson et al. (2006), will yield insight to these important issues.

7. Acknowledgements

The authors would also like to express sincere thanks the National Oceanic and Atmospheric Administration for funding this project through the Saltonstall-Kennedy program under Grant NAO3NMF4270183. In addition, this project could not have conducted without the operational and management staff at Heritage Salmon that operated the site during this study. Special appreciation goes to P. Lader, C. Stevens and T.H. Kim for their valuable input. Additional thanks go to G. McGillicuddy, G. Rice, C. Turmelle and O. Patursson for technical assistance and Professors B. Celikkol and K.C. Baldwin for advice and support.

8. References

Aarnses, J.V, Rudi, H., Loland G., 1990. Current forces on cage, net deflection. Engineering for Offshore Fish Farming. Thomas Telford, London pp 137-152.

Choo,Y.I., Casarella, M.J., 1971. Hydrodynamic resistance of towed cables. J. Hydronautics. 126-131.

Fredriksson, D.W., DeCew, J.C., Tsukrov, I. (in preparation). Development of structural models for evaluating HDPE plastic net pens used in marine aquaculture.

Fredriksson, D.W., DeCew, J.C., Irish, J.D. 2006. A field study to understand the currents and loads of a near shore fish farm. Proceedings of the Oceans 2006 MTS/IEEE Conference. Boston, MA. September 19, 2006.

Fredriksson, D.W., Swift, M.R., Eroshkin, O., Tsukrov, I., Irish, J.D., Celikkol, B. 2005. Moored fish cage dynamics in waves and currents. IEEE J. Oceanic. Eng. Vol. 30, No. 1 pp 28-36.

Fredriksson, D.W., DeCew, J., Swift, M.R., Tsukrov, I., Chambers, M.D., Celikkol, B. 2004. The Design and Analysis of a Four-Cage, Grid Mooring for Open Ocean Aquaculture. Aqua. Eng. Vol 32, No. 1 pp 77-94.

Fredriksson, D.W., Swift, M.R., Irish, J.D., Tsukrov, I., Celikkol, B. 2003a. Fish cage and mooring system dynamics using physical and numerical models with field measurements. Aqua. Eng. Vol 27, No. 2, pp. 117-146.

Fredriksson, D.W., Palczynski, M.J., Swift, M.R., Irish, J.D., Celikkol, B. 2003b. Fluid dynamic drag of a central spar cage in C.J. Bridger and B.A. Costa-Pierce, editors. Open Ocean Aquaculture: From Research to Commercial Reality. The World Aquaculture Society, Baton Rouge, Louisiana, United States. pp 151-168.

Gosz, M., Kestler, K., Swift, M.R. and Celikkol, B. 1996. Finite Element Modeling of Submerged Aquaculture Net-pen Systems. In: Open Ocean Aquaculture. Proceedings of an International Conference. May 8 – 10, 1996, Portland, Maine, Marie Polk, Ed. New Hampshire/Maine Sea Grant College Program Rpt. #UNHMP-CP-SG-96-9, 523-554.

Haritos, N. and He, D.T., 1992. Modelling the response of cable elements in an ocean environment. Finite Elements in Analysis and Design. 19, 19-32.

Loland, G. 1991. Current forces on and flow through fish farms. Ph.D. Thesis, Division of Marine Hydrodynamics at the Norwegian Institute of Technology. p. 149.

Morison, J.R., Johnson, J.W., O'Brien, M.P., Schaaf, S.A. 1950. The forces exerted by surface waves on piles. Petroleum Transactions, American Inst. of Mining Eng. Vol 189, pp 149-157.

Palczynski, M.J. 2000. Fish Cage Physical Modeling. Master's Degree Thesis submitted in partial requirement for the Ocean Engineering degree program. University of New Hampshire, Durham, NH.

Patursson, O., Swift, M.R., Baldwin, K., Tsukrov, I., Simonsen K. 2006. Modeling flow through and around a net panel using computational fluid dynamics. Proceedings of the Oceans 2006 MTS/IEEE Conference. Boston, MA. September 19, 2006.

Plew, D.R., Stevens, C.L., Spigel, R.H., Hartstein, N.D., 2005. Hydrodynamic implications of large offshore mussel farms. IEEE J. Oceanic. Eng. Vol. 30, No. 1, pp 95-108.

Rice, G., Boduch, S., DeCew, J., Irish, J.D., Swift, M.R., Turmelle, C.A. 2006. An investigation of a deployed submerged grid mooring system. Proceedings of the Oceans 2006 MTS/IEEE Conference. Boston, MA. September 19, 2006.

Tsukrov, I, Eroshkin, O., Paul, W., Celikkol, B. 2005. Numerical modeling of nonlinear elastic components of mooring systems. IEEE J. Oceanic. Eng. Vol. 30, No. 1 pp 37-46.

Tsukrov, I., Eroshkin, O., Fredriksson, D. W., Swift, M.R., Celikkol, B. 2003. Finite element modeling of net panels using consistent net element. Ocean Eng. 30: pp. 251 – 270.

Table 1

The current velocities measured at the external location of the farm for the clean and fouled net conditions.

Net condition	Date	Time (UTC)	Magnitude (m/s)	Direction (degrees)	East-going (m/s)	North-going (m/s)
Clean	7/28/04	2040	0.276	328	-0.147	0.233
		2100	0.271	347	-0.063	0.264
		2120	0.304	333	-0.138	0.271
		Ave[1]	-	-	-0.101	0.267
Fouled	10/28/03	0140	0.264	331	-0.125	0.232
		0200	0.236	344	-0.065	0.227
		0220	0.248	308	-0.196	0.153
		Ave[1]	-	-	-0.131	0.190

[1]Represents the average between on the hour and 20 minutes past the hour measurements

Table 2

The estimated variance and RMS velocities calculated from the tidal currents at each location for the three net conditions.

	Smolt nets	Clean nets	Fouled nets
External Velocity Variance $(m/s)^2$	0.057	0.045	0.051
Internal Velocity Variance $(m/s)^2$	0.028	0.028	0.009
External U_{RMS} (m/s)	0.239	0.211	0.227
Internal U_{RMS} (m/s)	0.160	0.167	0.093
Percent Reduction	71	79	41

Table 3

The velocity reduction values used as input to the numerical model

Net condition	Date and Time (UTC)	Position	Speed (m/s)	East-going (m/s)	North-going (m/s)
Clean	07/28/04 2100 - 2120	Outside	0.286	-0.101	0.267
		One Pen	0.227	-0.080	0.213
		Two Pens	0.182	-0.064	0.170
		Three Pens	0.144	-0.051	0.134
Fouled	10/28/03 0200 - 0220	Outside	0.231	-0.131	0.190
		One Pen	0.096	-0.054	0.079
		Two Pens	0.040	-0.022	0.033
		Three Pens	0.016	-0.009	0.013

Table 4

The net twine diameter and spacing characteristics for each net condition (net solidity information is also included)

	Smolt net condition	Clean net condition	Fouled net condition
Predator net			
Twine diameter (mm)	3.25	3.25	3.25
Knot-to-knot spacing (mm)	102	102	102
Solidity (%)	6.4	6.4	n.a.[1]
Fish (containment) net			
Twine diameter (mm)	-	2.0	2.0
Knot-to-knot spacing (mm)	-	30.2	30.2
Solidity (%)	-	13.3	n.a.[1]
Smolt Net			
Twine diameter (mm)	3	-	-
Knot-to-knot spacing (mm)	17.5	-	-
Solidity (%)	34.4	-	-
Total net solidity (%)	40.8	19.7	58.8

[1]Only the total solidity of the fouled net condition was estimated.

Table 5

Numerical model geometric and material properties for the net pen

Component	Parameter	Value
Cage rim[1]	Modulus of elasticity	1.172 x 10^9 Pa
	Density	289 kg/m^3
	Cross sectional area	0.082 m^2
Ballast rim[2]	Modulus of elasticity	1.172 x 10^9 Pa
	Density	1739 kg/m^3
	Cross sectional area	0.022 m^3
Net[3]	Modulus of elasticity[6]	2.0 x 10^9 Pa
	Density[5]	1025 m^3
	Cross sectional area	4.55 x 10^{-6} m^2
	Representative solidity	19.7 %
Net[4]	Modulus of elasticity[6]	2.0 x 10^9 Pa
	Density[5]	1025 m^3
	Cross sectional area	7.354 x 10^{-6} m^2
	Representative solidity	58.8 %

[1] Rim and stanchion components are modeled as a single rim
[2] Ballast rim is filled with sand
[3] Estimated combined solidity for clean nets
[4] Estimated combined solidity for fouled nets
[5] Net was assumed to be neutrally buoyant
[6] Representative modulus of elasticity was used

Table 6

Numerical model geometric and material properties for the mooring system

Component	Parameter	Value
Anchor chain (1 to 1-1/2" long link)	Modulus of elasticity	2.0×10^{11} Pa
	Density	8655 kg/m^3
	Cross sectional area	3.366×10^{-3} m^2
Connector plate (1" steel plate)	Modulus of elasticity	2.0×10^{11} Pa
	Density	6920 kg/m^3
	Cross sectional area	1.01×10^{-2} m^2
Grid line (three-strand co-polymer)	Modulus of elasticity	8.559×10^{9} Pa
	Density	963.5 kg/m^3
	Cross sectional area	2.027×10^{-3} m^2
Buoy chain (steel)	Modulus of elasticity	2.0×10^{11} Pa
	Density	8684 kg/m^3
	Cross sectional area	8.416×10^{-4} m^2
Buoy (steel ball)	Modulus of elasticity	2.0×10^{11} Pa
	Density	212.1 kg/m^3
	Cross sectional area	1.674 m^2
Net pen attachment line (three-strand co-polymer)	Modulus of elasticity	9.27×10^{9}Pa
	Density	963.5 kg/m^3
	Cross sectional area	7.917×10^{-4} m^2

Table 7

The mean and maximum values obtained from the SW-S and South anchor leg load cell data sets (also included are the calculated results with and without velocity reduction from the numerical model)

			Measured		Calculated	
Net Condition	Date and Time (UTC)	Anchor Position	Mean value (kN)	Maximum value (kN)	Velocity reduction (kN)	No reduction (kN)
Clean	7/28/04 2100	SW-S	14.6	17.3	16.3	22.7
		South	24.5	29.2	34.5	55.5
Fouled	10/18/03 0200	South	21.1	39.1	22.4	58.9

Figure 1: The Broad Cove fish farm is located in the state of Maine (USA).

Figure 2: A schematic of the fish farm in Broad Cove (plan view). The farm contains 20 net pens. Field instruments were deployed around the southwest net pen. Each net pen has a circumference of 100 meters.

Figure 3: Locations of the instruments installed on the southwest corner of the fish farm. Note that the individual components of the grid mooring are not to scale.

Figure 4: Load cell data results from the clean (South and SW-S anchor) and fouled (South anchor) net conditions.

Figure 5: The stepwise horizontal velocity reduction through the farm. The flow encounters the farm at a 45 degree angle. Reduction is given for the smolt, clean and fouled net conditions.

Figure 6: Numerical model predictions of mooring tension (in kN) for the clean net condition (July 28, 2004 at 2100 UTC). Bold and underlined values are the results with and without employing velocity reduction, respectively. The current velocity vector components are also shown.

Figure 7: Numerical model predictions of mooring tension (in kN) for the fouled net condition (October 28, 2003 at 0200 UTC). Bold and underlined values are the results with and without employing velocity reduction, respectively. The current velocity vector components are also shown.

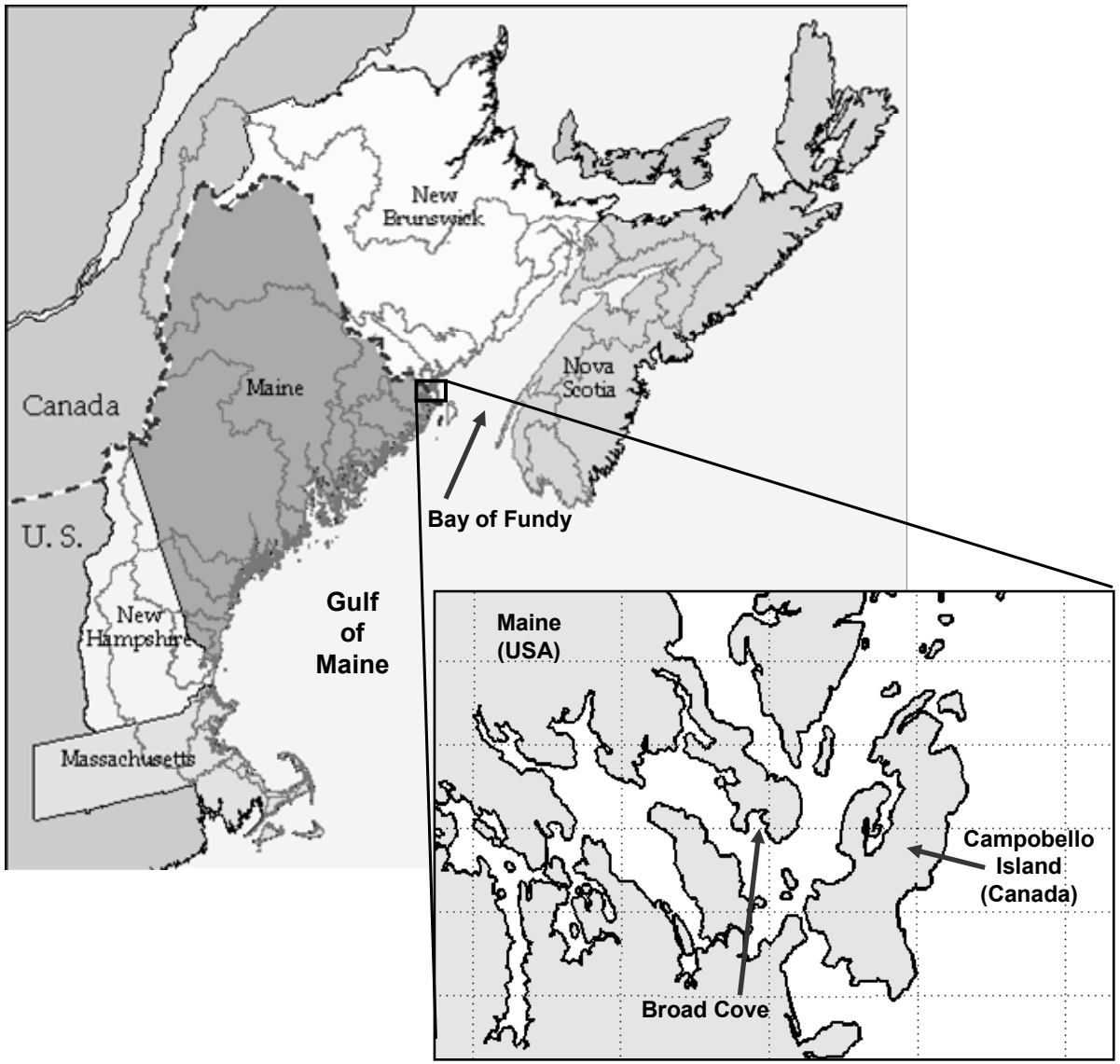

Figure 1
D.W. Fredriksson

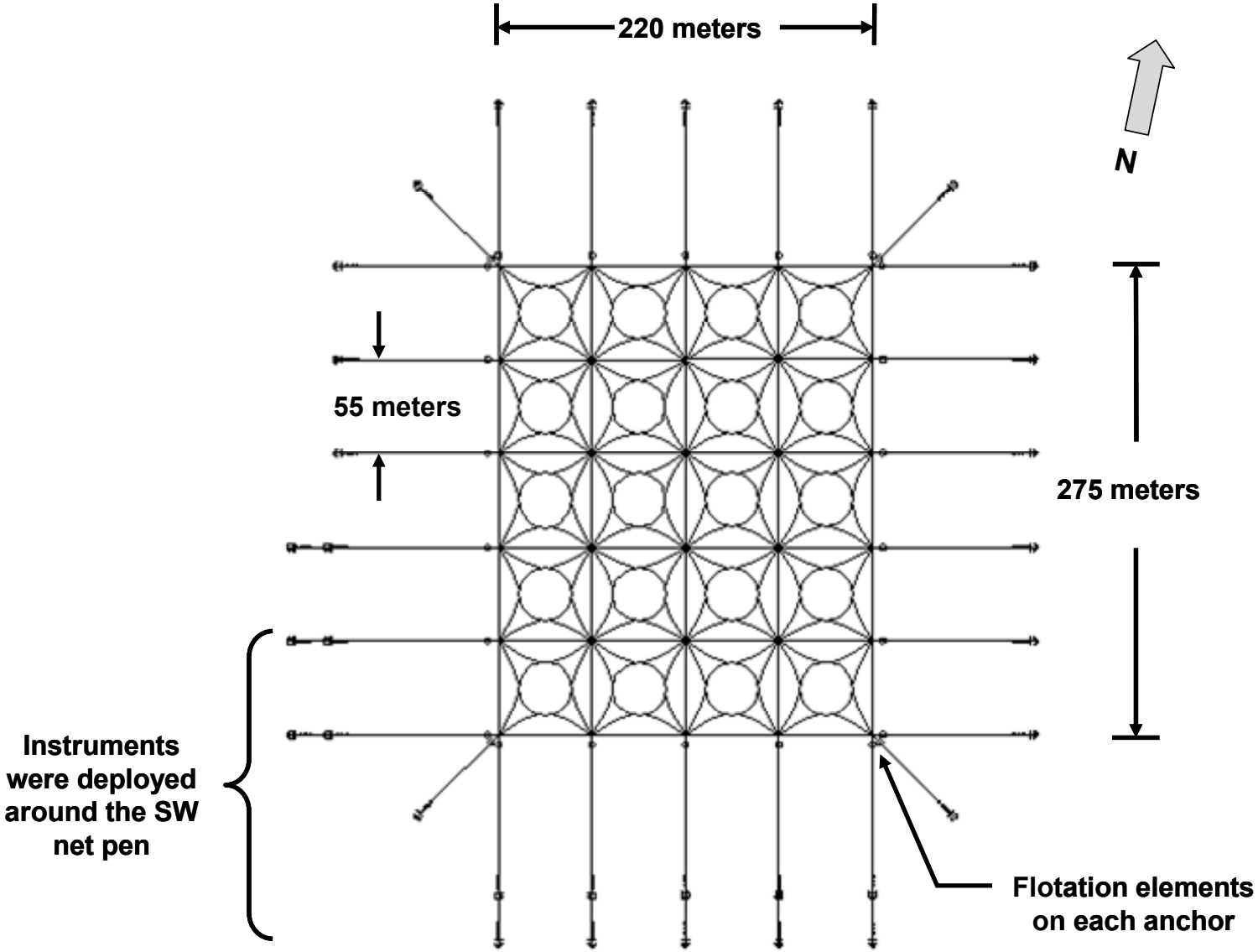

Figure 2
D.W. Fredriksson

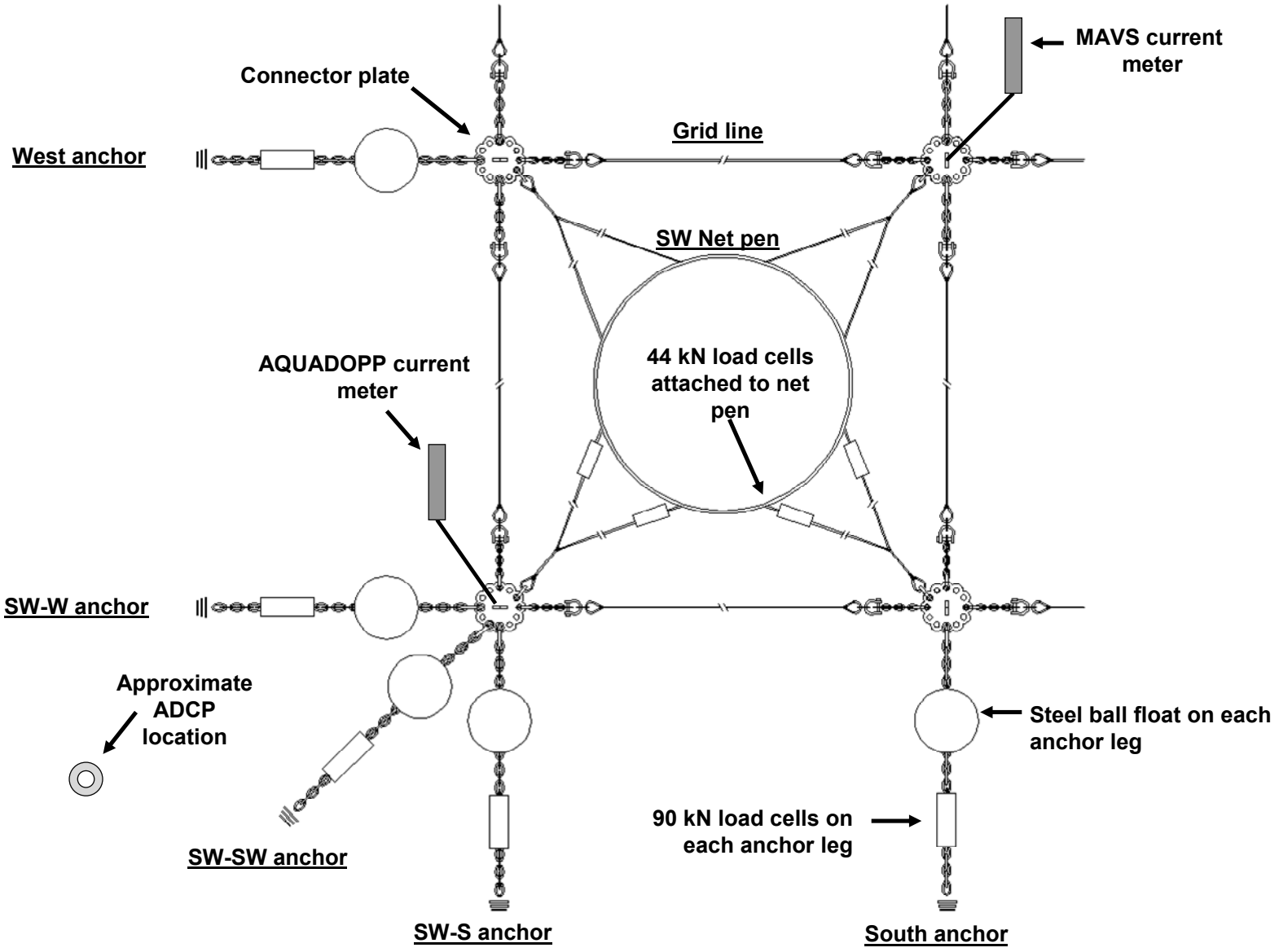

Figure 3
D.W. Fredriksson

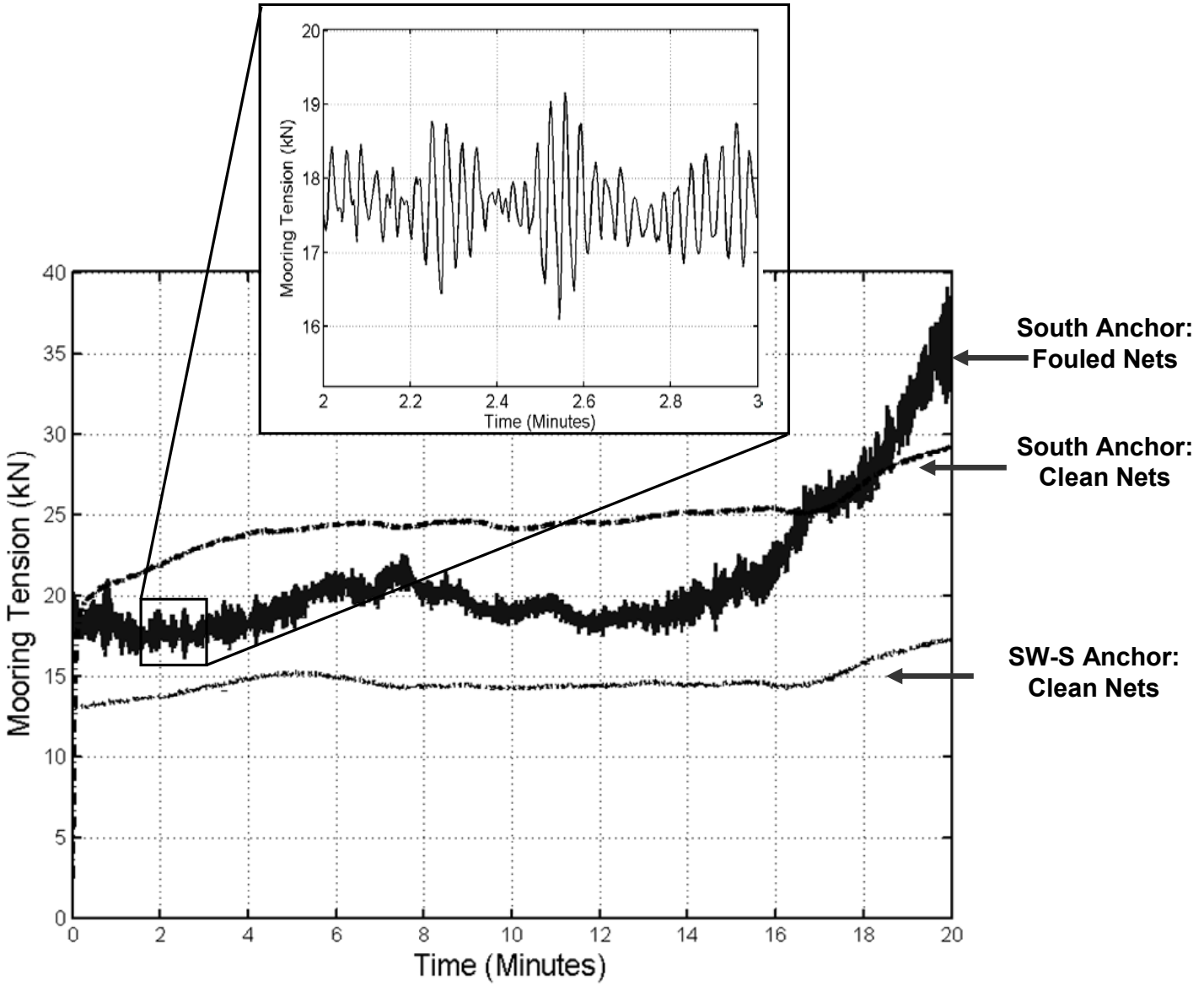

Figure 4
D.W. Fredriksson

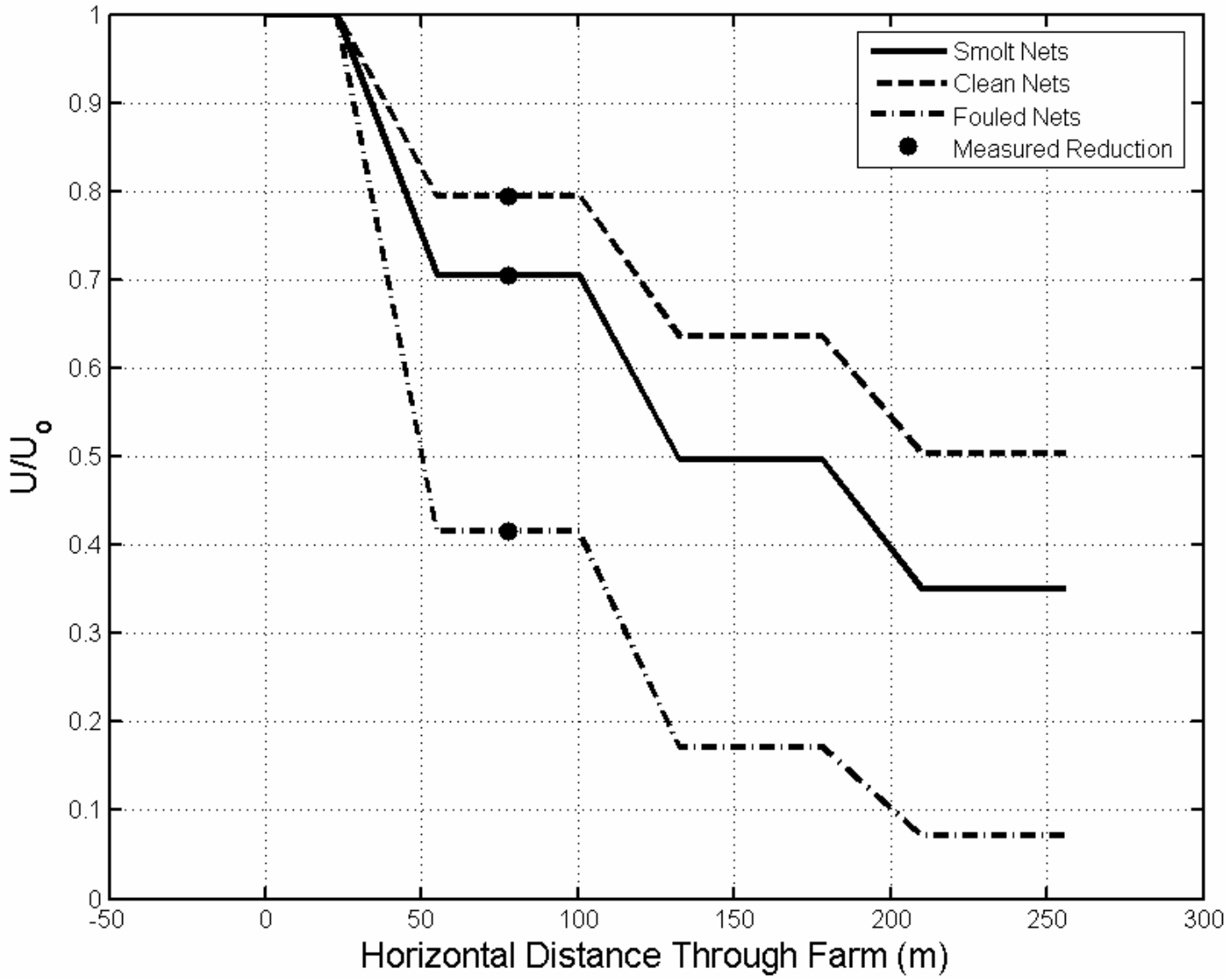

Figure 5
D.W. Fredriksson

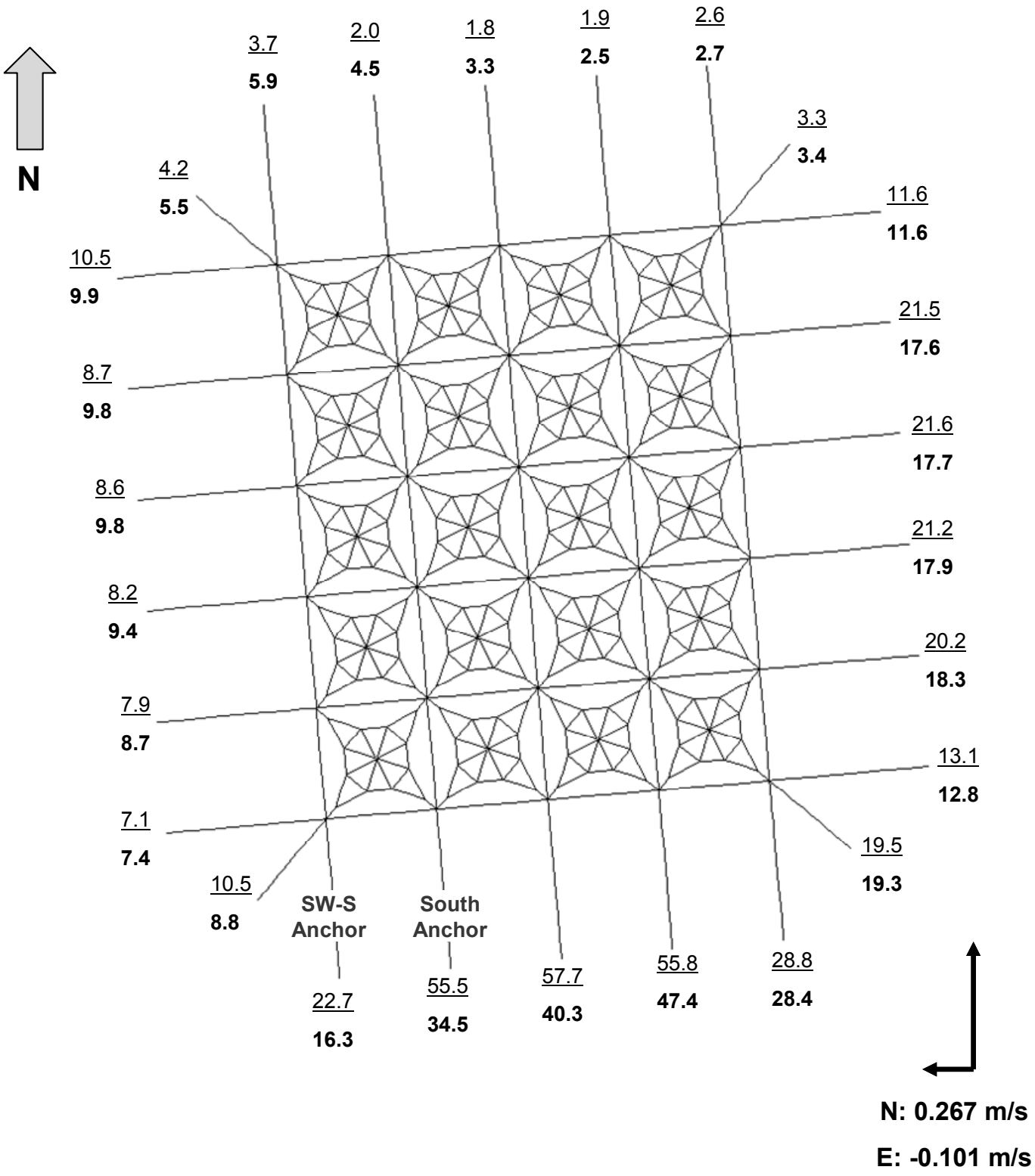

Figure 6
D.W. Fredriksson

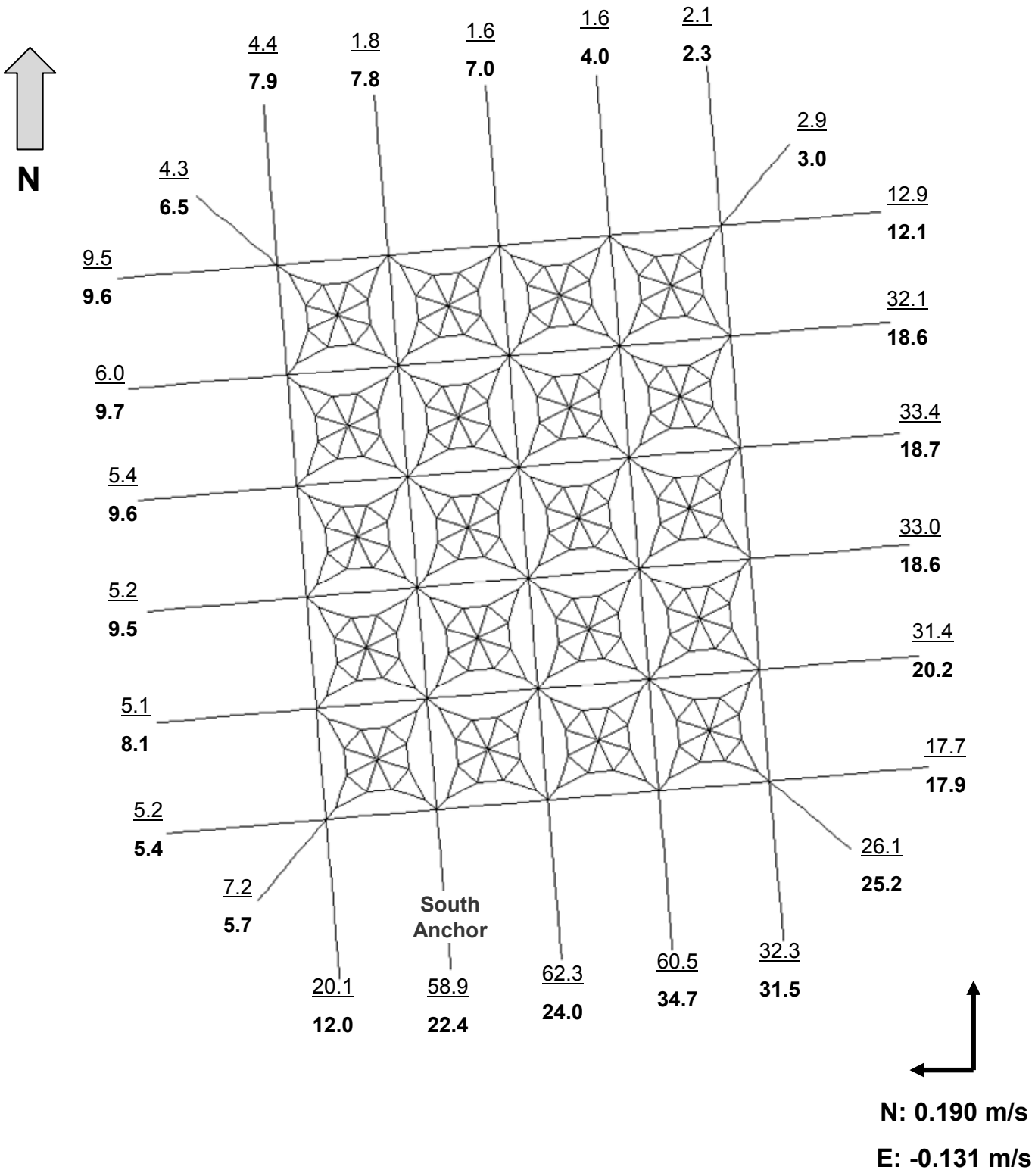

Figure 7
D.W. Fredriksson